

Monte Carlo Renormalization Group Analysis of Lattice ϕ^4 Model in $D = 3, 4$

M. Itakura

*Center for Promotion of Computational Science and Engineering, Japan Atomic Energy Research
Institute, Meguro-ku, Nakameguro 2-2-54, Tokyo 153, Japan*

(June 25, 2021)

Abstract

We present a simple, sophisticated method to capture renormalization group flow in Monte Carlo simulation, which provides important information of critical phenomena. We applied the method to the $D = 3, 4$ lattice ϕ^4 model and obtained a renormalization flow diagram that well reproduces theoretically predicted behavior of the continuum ϕ^4 model. We also show that the method can be easily applied to much more complicated models, such as frustrated spin models.

PACS numbers: 02.70.Lq, 75.10.Hk

I. INTRODUCTION

Renormalization-group (RG) theory [1–4] has drastically improved our perspective about phase transition. When it is combined with Monte Carlo (MC) simulations, it becomes a very powerful tool to investigate critical phenomena. However, the so-called Monte Carlo renormalization group (MCRG) method [5–9] requires an elaborate scheme and experience, and application has been restricted to simple models such as the Ising ferromagnet up to now. In this paper we reformulate the MCRG method and present a simple way to obtain the RG flow diagram in a MC simulation, which can provide essential information about critical phenomena. This paper is organized as follows. In Sec. II, problems in the conventional MCRG scheme are explained and remedies for each problem are presented. In fact, modification of the conventional scheme leads to use of Binder’s parameter [10] and the second parameter, which is used in recent high-precision numerical analyses [15,14]. In Sec. III, expected behavior of RG flow in the $D = 4$ lattice ϕ^4 model is presented for comparison with the MC result. Some caution on MC simulation just at the upper critical dimension is also presented. In Sec. IV, details of the MC simulation of the lattice ϕ^4 model are described. In Sec. V and VI, results of the MC simulation for $D = 3, 4$ are presented. In Sec. VII, we summarize the result and discuss possible applications of the method to more complicated models.

II. MODIFICATION OF THE CONVENTIONAL MCRG METHOD

In the conventional MCRG scheme [5–8], critical exponents are calculated from eigenvalues of the linearized RG transformation:

$$\frac{\partial K_i(L, b_1)}{\partial K_j(L, b_2)} \quad (1)$$

where $K_i(L, b)$ denotes coupling strength of the i 'th term of a block-spin Hamiltonian with block size b , and L denotes the original size of the system.

One problem is that one should use the proper definition of block spin, otherwise $K_i(L, b)$ goes to zero or infinity as b becomes large even at the critical point. For the Ising model, the majority rule is one of the options. However, it cannot be extended to more complicated models. There are infinite kinds of definitions and location of the fixed point (along an irrelevant direction) depends on it [6].

In this paper, we use one that seems most simple and suitable for Monte Carlo simulation,

$$\bar{s}_b \equiv s_b / \sqrt{\langle s_b^2 \rangle}, \quad (2)$$

where s_b denotes summation of all spins in the block. This definition is implicitly used in the definition of Binder’s parameter. Actually, we use coarse-grained spin obtained by cutting high-momentum modes off, as in Ref. [9]. However, we set $b = L$ at the last stage, therefore real-space RG and momentum-space RG do not make much difference.

Another problem is that the block size b should be much smaller than L , otherwise the behavior of the block spin is affected by a boundary condition that is nonuniversal. Thus one

faces a tradeoff that for larger b , behavior of block spins become more asymptotic (couplings of irrelevant terms become smaller) but their behavior deviates from bulk one. The solution is to use the following matrix

$$\frac{\partial K_i(bL, bL)}{\partial K_j(L, L)} = \frac{\partial K_i(bL, bL)}{\partial K_j(bL, b)} \cdot \frac{\partial K_i(bL, b)}{\partial K_j(bL, 1)} \cdot \left[\frac{\partial K_i(L, L)}{\partial K_j(L, 1)} \right]^{-1}, \quad (3)$$

instead of (1). At the critical point,

$$\frac{\partial K_i(bL, bL)}{\partial K_j(bL, b)} = \frac{\partial K_i(L, L)}{\partial K_j(L, 1)} \quad (4)$$

should be satisfied and eigenvalues of the matrix (3) coincide with that of (1). Thus one can use as large a block size as the system size.

Yet another, and most severe problem, is referred to as the "redundancy problem" [7,8]. In the conventional MCRG scheme, one should observe very large numbers of block-spin interaction terms to construct a fixed-point Hamiltonian. However, in the continuum ϕ^4 theory, there are only two kinds of independent coupling constants (mass and coupling). The lattice Hamiltonian approaches this continuum asymptotically after the momentum-space RG transformation, and the two terms are enough to observe essential RG flow.

Let us consider the Hamiltonian defined on D -dimensional continuum space:

$$\mathcal{H} = \int d\mathbf{x} \left[\frac{\gamma}{2} [\nabla\phi(\mathbf{x})]^2 + \frac{\alpha}{2}\phi(\mathbf{x})^2 + \beta\phi(\mathbf{x})^4 \right]. \quad (5)$$

Note that it is not a microscopic Hamiltonian: it is a phenomenological Hamiltonian and the parameters γ, α, β should be determined to reproduce experimental results. In other words, it is the logarithm of probability of observing a specific configuration of some physical quantity $\phi(\mathbf{x})$ in the experiment. This means that short length scale fluctuations beneath the resolution l of the observation device are already integrated out and absorbed into the parameters γ, α, β . Thus parameters depend on the cutoff length l and should be denoted by $\gamma_l, \alpha_l, \beta_l$. We also denote the physical quantity $\phi(\mathbf{x})$ averaged over a volume of linear length l by $\phi_l(\mathbf{x})$.

We replace the parameters in (5) by "regularized" ones defined as follows:

$$\bar{\alpha}_l = l^D \langle \phi_l(x)^2 \rangle \alpha_l, \quad \bar{\beta}_l = l^D \langle \phi_l(x)^2 \rangle^2 \beta_l, \quad \bar{\gamma}_l = l^{D-2} \langle \phi_l(x)^2 \rangle \gamma_l.$$

In terms of this regularization, the Hamiltonian is expressed as

$$\int_{|\mathbf{p}| \leq \pi} d\mathbf{p} \frac{\bar{\alpha} + \bar{\gamma}\mathbf{p}^2}{2} \bar{\phi}(\mathbf{p}) \bar{\phi}(-\mathbf{p}) + \bar{\beta} \int_{|\mathbf{p}_i| < \pi} d\mathbf{p}_1 d\mathbf{p}_2 d\mathbf{p}_3 d\mathbf{p}_4 \delta\left(\sum_i \mathbf{p}_i\right) \bar{\phi}(\mathbf{p}_1) \bar{\phi}(\mathbf{p}_2) \bar{\phi}(\mathbf{p}_3) \bar{\phi}(\mathbf{p}_4), \quad (6)$$

where $\bar{\phi}(\mathbf{p}) \equiv \phi(\mathbf{p}l) \langle \phi_l^2 \rangle^{-1/2}$. All possible values of the regularized parameter fall on a two-dimensional manifold on which $\langle \bar{\phi}_l(x)^2 \rangle = 1$ is satisfied. This regularization is suitable for MC simulations, compared to the field theoretical one, $\gamma \equiv 1$. Figure 1 and Fig.2 show schematic RG flow of these regularized parameters in $D = 3$ and 4, respectively:

high temperature, low temperature, Gaussian, and Wilson-Fisher fixed point are denoted by H,L,G, and WF, respectively.

Now let us return to the lattice model defined as follows:

$$H_L = \frac{\gamma}{2} \sum_{\langle ij \rangle} (s_i - s_j)^2 + \sum_i \frac{\alpha}{2} s_i^2 + \beta s_i^4. \quad (7)$$

where the summation $\sum_{\langle ij \rangle}$ sums over all nearest neighbor pairs. If we apply the momentum-space RG transform of factor b to (7), the renormalized Hamiltonian takes the following form:

$$H(L, b) = \frac{\bar{\alpha}(L, b)}{2} (L/b)^{-D} \sum_{|\mathbf{p}| \leq \pi}^{(L/b)} \bar{s}_b(\mathbf{p}) \bar{s}_b(-\mathbf{p}) \quad (8)$$

$$+ \frac{\bar{\gamma}(L, b)}{2} (L/b)^{-D} \sum_{|\mathbf{p}| \leq \pi}^{(L/b)} \mathbf{p}^2 \bar{s}_b(\mathbf{p}) \bar{s}_b(-\mathbf{p}) \quad (9)$$

$$+ \bar{\beta}(L, b) (L/b)^{-3D} \sum_{\substack{|\mathbf{p}_i| \leq \pi \\ \mathbf{p}_1 + \mathbf{p}_2 + \mathbf{p}_3 + \mathbf{p}_4 = 0}}^{(L/b)} \bar{s}_b(\mathbf{p}_1) \bar{s}_b(\mathbf{p}_2) \bar{s}_b(\mathbf{p}_3) \bar{s}_b(\mathbf{p}_4), \quad (10)$$

where $\bar{s}_b(\mathbf{p}) = s(b\mathbf{p}) < s_b^2(x) >^{-1/2}$ and the symbol $\sum_{\mathbf{p}}^{(N)}$ denotes summation over $0, \pm 2\pi/N, \pm 4\pi/N, \dots$, for each component of \mathbf{p} , $s(\mathbf{p})$ denotes Fourier components of s_i , and

$$s_b(\mathbf{x}) = (L/b)^{-D} \sum_{|\mathbf{p}| \leq \pi/b} e^{i\mathbf{p} \cdot \mathbf{x}} s(\mathbf{p}) \quad (11)$$

is coarse-grained spin at \mathbf{x} . Actually, higher terms such as $O(\bar{s}_b^6)$ are present in $H(L, b)$ but they vanish as L and b become large.

Note that $\langle \sum_{\mathbf{p}} \bar{s}_b(\mathbf{p}) \bar{s}_b(-\mathbf{p}) \rangle = \text{const}$ by definition and there are only two kinds of interesting terms. If we set $b = L$, the term (10) is exactly the Binder's parameter and we denote it by B_L . The term (9) vanishes if we set $b = L$, so we must stop RG transform at $b = L/2$. Then it becomes

$$\frac{2\pi^2 \langle s(\mathbf{k}_1) s(-\mathbf{k}_1) \rangle}{2^{-D} \langle s(0)^2 + 2s(\mathbf{k}_1) s(-\mathbf{k}_1) \rangle}, \quad (12)$$

where $\mathbf{k}_1 \equiv (2\pi/L, 0, \dots, 0)$. For simplicity, we use the following quantity:

$$C_L \equiv \frac{\langle s(\mathbf{k}_1) s(-\mathbf{k}_1) \rangle}{\langle s^2(0) \rangle}. \quad (13)$$

Recently, several different parameters have been proposed as the second parameter C_L to estimate and eliminate the subleading scaling field. We will review these works in Sec.II A.

Now consider the following matrix:

$$\frac{\partial(B_{bL}, C_{bL})}{\partial(B_L, C_L)} = \frac{\partial(B_{bL}, C_{bL})}{\partial(\bar{\beta}_1, \bar{\gamma}_1)} \cdot \left(\frac{\partial(B_L, C_L)}{\partial(\bar{\beta}_1, \bar{\gamma}_1)} \right)^{-1} \quad (14)$$

$$= \frac{\partial(B_{bL}, C_{bL})}{\partial(\bar{\beta}_b, \bar{\gamma}_b)} \cdot \frac{\partial(\bar{\beta}_b, \bar{\gamma}_b)}{\partial(\bar{\beta}_1, \bar{\gamma}_1)} \cdot \left(\frac{\partial(B_L, C_L)}{\partial(\bar{\beta}_1, \bar{\gamma}_1)} \right)^{-1} \quad (15)$$

instead of

$$\frac{\partial[\bar{\beta}(bL, bL), \bar{\gamma}(bL, bL/2)]}{\partial[\bar{\beta}(L, L), \bar{\gamma}(L, L/2)]}. \quad (16)$$

At the fixed point,

$$\frac{\partial(B_L, C_L)}{\partial(\bar{\beta}_1, \bar{\gamma}_1)} = \frac{\partial(B_{bL}, C_{bL})}{\partial(\bar{\beta}_b, \bar{\gamma}_b)} \quad (17)$$

is satisfied and eigenvalues of $\partial(B_{bL}, C_{bL})/\partial(B_L, C_L)$ coincide with that of $\partial(\bar{\beta}_b, \bar{\gamma}_b)/\partial(\bar{\beta}_1, \bar{\gamma}_1)$ as long as $\partial(B_L, C_L)/\partial(\bar{\beta}_1, \bar{\gamma}_1)$ is a nonsingular matrix.

Thus scaling behavior of renormalized parameters can be extracted from that of (B_L, C_L) , as long as $|\partial(B_L, C_L)/\partial(\bar{\beta}_1, \bar{\gamma}_1)| \neq 0$: If we draw arrows from (B_L, C_L) to (B_{bL}, C_{bL}) in the B_L - C_L plane, the renormalization flow diagram of factor b is obtained. From this diagram, one can determine whether the MC result is asymptotic enough or not, by checking whether (B_L, C_L) converge to a fixed point. When a subleading scaling field is expected to be very large, such as in the recent Monte Carlo studies of five-dimensional (5D) Ising model [11–13], this RG flow diagram is very useful compared to a many parameter fit to a single observable B_L .

A linearized RGT matrix $\mathbf{R}_b = \partial(B_{bL}, C_{bL})/\partial(B_L, C_L)$ is calculated, for example, from linear fitting

$$\begin{pmatrix} B_{bL}(\alpha, \beta, \gamma) \\ C_{bL}(\alpha, \beta, \gamma) \end{pmatrix} = \mathbf{R}_b \begin{pmatrix} B_L(\alpha, \beta, \gamma) \\ C_L(\alpha, \beta, \gamma) \end{pmatrix} + \begin{pmatrix} B_0 \\ C_0 \end{pmatrix}, \quad (18)$$

where \mathbf{R}_b and (B_0, C_0) are fitting parameters and we use values of (B_L, C_L) and (B_{bL}, C_{bL}) at several different parameters α, β, γ near the fixed point. Selection of this parameter is a delicate problem: when it is too close to the fixed point, (B_L, C_L) and (B_{bL}, C_{bL}) become very close to each other and the RG flow is buried in statistical errors, while when it is far from the fixed point, nonlinear dependence of (B_L, C_L) on (α, β, γ) induces a systematic error. Thus the parameter range for the fitting should be determined carefully.

Of course \mathbf{R}_b can be calculated from α, β, γ derivatives of B_L and C_L at the fixed point. However, derivatives with respect to irrelevant direction vanish as L becomes large and buried in statistical errors. Thus values of B_L, C_L at parameters well apart from the fixed point along an irrelevant direction are needed to calculate the second eigenvalue.

A. The second parameter in literature

Here we compare our definition of C_L , “the second parameter” (the first one is the Binder’s parameter), with preceding works.

Ballesteros *et al.* [14] used a finite-size correlation length defined below as

$$\xi^2 \equiv \frac{\langle \phi(0)^2 \rangle / \langle \phi(\mathbf{k}_1)\phi(-\mathbf{k}_1) \rangle - 1}{\sin^2(|\mathbf{k}_1|)}, \quad (19)$$

which is related to C_L as $\xi^2 \sin^2(|\mathbf{k}_1|) = -1 + 1/C_L$.

Hasenbusch [15] used the ratio between the partition function of a periodic and antiperiodic Hamiltonian. In momentum representation, the Hamiltonian for an antiperiodic boundary condition (APBC) is obtained by replacing \mathbf{k} summation of the lattice Hamiltonian by $k_\mu = \pm\pi/L, \pm 3\pi/L, \dots$ for each direction μ to which the APBC is imposed. Let us denote the partition function of a periodic and antiperiodic Hamiltonian by Z_p and Z_a , respectively. It then reads:

$$Z_a/Z_p = \frac{\int \mathcal{D}\phi \exp(-H_a)}{\int \mathcal{D}\phi \exp(-H_p)} \quad (20)$$

$$= \frac{\int \mathcal{D}\phi \exp(-H_p) \exp(H_p - H_a)}{\int \mathcal{D}\phi \exp(-H_p)} = \langle \exp(H_p - H_a) \rangle_p \quad (21)$$

where H_p and H_a denote the periodic and antiperiodic Hamiltonian, respectively, $\langle \dots \rangle_p$ denotes average with respect to H_p . When the APBC is imposed to a direction of \mathbf{e}_1 , it reads

$$H_a - H_p \sim \sum_{\mathbf{k}} \frac{2\pi|k_1|}{L} \phi(\mathbf{k}) \phi(-\mathbf{k}) \quad (22)$$

for large L . One can see that Z_a/Z_p has a similar form as that of C_L . In the real-space RG scheme, both C_L and Z_a/Z_p can be regarded as an effective coupling between two block spins defined on $L \times L \times \dots \times L/2$ block.

III. PERTURBATION EXPANSION AT $D = 4$

Near the Gaussian fixed point, finite-size behavior of B_L and C_L can be predicted from finite-size perturbation theory proposed by Chen and Dohm [16]. Note that, when $D = 4$, there is one kind of divergent subdiagram (Fig. 3) whose factor is proportional to $[\beta_1(C_0 + C_1 \ln L)/\gamma_1^2]$ at the critical region, where $C_0, C_1 > 0$ are some constants. Thus perturbation is restricted to the range $\beta_1(C_0 + C_1 \ln L)/\gamma_1^2 \ll 1$ and one cannot set $L \rightarrow \infty$. However, the limit for L rapidly diverges as we approach the Gaussian fixed point, and good agreement between perturbation theory and Monte Carlo data is expected for a certain parameter range and lattice size. Then one can predict scaling behavior for large L , which is far beyond the computational limit of Monte Carlo simulation, from the perturbation theory.

Here we investigate finite-size behavior of B_L and C_L at the finite-size critical point (to one-loop order):

$$\alpha = -12 \frac{\beta}{\gamma} L^{-D} \sum_{\mathbf{k} \neq 0} \frac{1}{2J(\mathbf{k})} \quad (23)$$

where $J(\mathbf{k}) = \sum_{\mu} (1 - \cos k_{\mu})$.

B_L takes the so-called zero-mode value:

$$B_{\text{ZM}} \equiv \frac{\int d\Phi_0 \exp(-\Phi_0^4) \Phi_0^4 / \int d\Phi_0 \exp(-\Phi_0^4)}{[\int d\Phi_0 \exp(-\Phi_0^4) \Phi_0^2 / \int d\Phi_0 \exp(-\Phi_0^4)]^2} \approx 2.1844. \quad (24)$$

As for C_L , to one-loop order,

$$C_L = \frac{\sqrt{\beta}}{8\pi^2\gamma} \sqrt{1 - 36 \frac{\beta}{\gamma^2} \sum_{\mathbf{k} \neq 0} [2J(\mathbf{k})]^{-2}}. \quad (25)$$

For large L , $\sum_{\mathbf{k} \neq 0} [2J(\mathbf{k})]^{-2} \sim A_1 + A_2 \ln L$ where A_1 and A_2 are some positive constant. Thus the plot of (B_L, C_L) for a certain range of parameters including critical temperature approaches $(B_{\text{ZM}}, 0)$ as L increases or β decreases, indicating that the Gaussian fixed point is infrared stable. However, approach to the point $(B_{\text{ZM}}, 0)$ for increasing L is extremely slow, and one cannot expect asymptotic Gaussian behavior in MC simulations, even when L is very large. Critical exponents estimated from MC results may also differ from the Gaussian (classical) value and depend on the bare parameters. Thus one can extract only very restricted information from MC simulations at the upper critical dimension.

IV. DETAIL OF MONTE CARLO SIMULATION

We investigated the $L \times L \times L$ system with $L = 8, 16, 32$ for $D = 3$ and the $L \times L \times L \times L$ system with $L = 4, 8, 16$ for $D = 4$, imposing a periodic boundary condition on each directions.

We used the following Hamiltonian:

$$H = \frac{\gamma}{2} \sum_{\langle ij \rangle} (s_i - s_j)^2 + \frac{\alpha}{2} \sum_i s_i^2 + \beta \sum_i s_i^4 \quad (26)$$

where $-\infty < s_i < \infty$ denotes the spin on the site i . Since we cannot use the regularization condition $\langle s_i^2 \rangle = 1$ before the simulation, we used the following one

$$\frac{\int d\phi \exp(-\frac{\alpha}{2}\phi^2 - \beta\phi^4) \phi^2}{\int d\phi \exp(-\frac{\alpha}{2}\phi^2 - \beta\phi^4)} = 1.$$

We used several fixed α, β and tuned γ to reach the critical region. Actual values of parameters are listed in the later sections.

For parameters well apart from the Gaussian fixed point, $4L^{D-2}$ single cluster flips [17] and 16 Metropolis sweeps are performed between successive observations. In the cluster-update stage, length of s_i is kept fixed and only its sign is changed. In the Metropolis update step, a new value for s_i is chosen uniformly from a range $\exp(-\alpha s^2 - \beta s^4) \geq \exp(-3.0)$. By the cluster update, all spins are flipped four times on average between observations. For all observed quantities, the correlation coefficient between successively observed values was less than 0.2.

As we approach the Gaussian fixed point, parameters behave as follows:

$$\alpha \sim 0, \quad \beta \sim \text{const}, \quad \gamma \rightarrow \infty. \quad (27)$$

Thus the nearest neighbor coupling $\gamma s_i s_j / 2$ tends to diverge. Since the bond-cutting probability of Wolff's algorithm is $\exp(-\gamma s_i s_j)$, the cluster update tends to end up with flipping

the whole system and does not accelerate the simulation. In these cases we increased the number of Metropolis sweeps until the above mentioned condition is satisfied.

Thermal averages of observables at γ slightly away from the actually used value were calculated using reweighting techniques [18]. For all system sizes, at least 0.8×10^5 observations were done after thermalization, and statistical errors were estimated by the jack-knife procedure. Multiplicative lagged Fibonacci sequence $R_t = R_{t-9689} \times R_{t-4187} \pmod{2^{31}}$ was used as a random number generator. All runs were performed on VPP-300 at JAERI.

V. RESULT FOR $D = 3$

Simulations were performed at the following parameters (see also Fig. 4) for $L = 8, 16, 32$;

Ising case: $\phi(\mathbf{x}) = \pm 1$, $\gamma = 0.2217$;

Case A: $\alpha/2 = -2.6159$, $\beta = 1.0948$, $\gamma = 0.3040$;

Case B: $\alpha/2 = -1.6655$, $\beta = 0.6935$, $\gamma = 0.3545$;

Case C: $\alpha/2 = -0.8786$, $\beta = 0.3938$, $\gamma = 0.4700$;

Case D: $\alpha/2 = -0.5209$, $\beta = 0.2713$, $\gamma = 0.6260$.

Figure 5 shows the RG flow diagram of B_L and C_L near the Wilson-Fisher RG fixed point. All lines are drawn from (B_L, C_L) to (B_{2L}, C_{2L}) . Dashed and solid lines correspond to $L = 8$ and $L = 16$, respectively. One can see that the RG flow shown in Fig. 1 is well reproduced. Moreover, the linear fitting procedure (18) provides an estimate for critical exponents as $\nu = 0.69(3)$, $\omega = 0.74(10)$ from $L = 8, 16$ data and $\nu = 0.653(10)$, $\omega = 0.7(2)$ from $L = 16, 32$ data, which is in agreement with the most recent ϵ -expansion result $\nu = 0.6305(25)$, $\omega = 0.814(10)$ [19] and the Monte Carlo result $\nu = 0.6296(3)$, $\omega = 0.845(10)$ [15]. Thus one can see that the two observables B_L and C_L are enough to capture the essential RG flow.

VI. RESULT FOR $D = 4$

Simulations were performed at the following parameters,

Ising case: $\phi(\mathbf{x}) = \pm 1$, $\gamma_1 = 0.1495$;

Case A: $\alpha/2 = -0.3226$, $\beta = 0.2082$, $\gamma = 0.54$;

Case B: $\alpha/2 = -0.1383$, $\beta = 0.1530$, $\gamma = 1.0$

for $L = 4, 8$, and 16 . Near the Gaussian fixed point (Case B), there is a severe, critical slowing down (owing to large fluctuation of the $\mathbf{k} = 0$ mode), which cannot be removed by the cluster update, and we did not perform $L = 16$ simulation. For Case B, perturbation expansion agrees well with the MC result: Fig.6(a) and 6(b) show the plot of B_L and C_L , respectively, against γ_1 for fixed (α, β) , together with perturbation results. Note that there

are no free parameters to be fitted, unlike the Ising case [20], and the agreement is both qualitative and quantitative.

Figure 7 shows a RG flow diagram of B_L and C_L obtained from MC simulations. All lines are drawn from (B_L, C_L) to (B_{2L}, C_{2L}) . Dashed and solid lines correspond to $L = 4$ and $L = 8$, respectively. Simulations at a parameter closer to the Gaussian fixed point than Case B are very difficult owing to aforementioned critical slowing down. Instead, finite-size perturbation provides reliable results near the Gaussian fixed point and it indicates that the plot of (B_L, C_L) approaches the Gaussian fixed point as L increases. Thus one can conclude that there is no RG fixed point except for the infrared-stable Gaussian fixed point.

VII. CONCLUSION

The renormalization-group flow diagram obtained by the method presented in this paper provides qualitative information such as the stability of a specific RG fixed point against some perturbation, as well as quantitative improvement of the estimated value of a critical exponent by eliminating leading correction-to-scaling terms. However, in lattice models, there exists $O(1/L)$ systematic error owing to the substitution of integral by finite summation of $1/L$ mesh, and one cannot get rid of this as long as the finite lattice system is concerned.

Our method can be easily extended to ϕ^4 models with several or unusual quartic coupling constant(s):

$$H = \int dx (\nabla\phi)^2 + \alpha\phi^2 + \sum_n \beta_n \sum_{ijkl} C_{ijkl}(n) \phi_i \phi_j \phi_k \phi_l, \quad (28)$$

such as the chiral $O(2n)$ model of a triangular antiferromagnet [21], and the Ginzburg-Landau model of a type-II superconductor under a weak or strong magnetic field, with or without point/columnar impurities (see [22,23] for transition of a pure system under a strong field). The multiple quartic term tends to generate an irrelevant operator whose correction exponent is very small, making it difficult to observe asymptotic behavior in MC simulations. Thus critical behavior of these models has been a controversial issue and application of the MCRG method to these models seems very interesting. A RG flow diagram of regularized quartic terms $\langle C_{ijkl}(n) \phi_i \phi_j \phi_k \phi_l \rangle / \langle \sum_i \phi_i^2 \rangle^2$ will reveal the critical behavior, as in Ref. [24] of the $Q = 4$ antiferromagnetic Potts model.

Another important problem is the estimation of the correction exponent for the ϕ^6 term at the WF fixed point. An ϵ expansion analysis indicates that it becomes positive at the WF fixed point [4]. However, whether the exponent is larger or smaller than $\omega \approx 0.8$ of ϕ^4 theory, which we assumed as a *leading* correction, should be confirmed numerically. Similarly, the effect of sixfold anisotropy on the critical behavior of a three-dimensional XY model is another interesting subject since the anisotropy is expressed by the $O(\phi^6)$ term.

REFERENCES

- [1] L.P.Kadanoff, *Physics* **2**, 263 (1966).
- [2] K.G.Wilson and J.Kogut, *Phys. Rep.* **12C**, 75 (1974).
- [3] D. J. Amit, *Field Theory, the Renormalization Group and Critical Phenomena*, 2nd. ed. (World Scientific 1984).
- [4] J. J. Binney, N. J. Dowrick, A. J. Fisher and M. E. J. Newman, *The Theory of Critical Phenomena* (Oxford University Press, Oxford, 1992).
- [5] R.H.Swendsen, *Phys. Rev. Lett.* **42**, 859 (1979).
- [6] H. W. J. Blöte, J. R. Heringa, A. Hoogland, E. W. Meyer, and T. S. Smit, *Phys. Rev. Lett.* **76**, 2613 (1996).
- [7] G. S. Pawley, R. H. Swendsen, D. J. Wallace, and K. G. Wilson, *Phys. Rev. B* **29**, 4030 (1984).
- [8] C. F. Baillie, R. Gupta, K. A. Hawick, and G. S. Pawley, *Phys. Rev. B* **45**, 10438 (1992).
- [9] D.Espriu and A.Travesset, *Phys. Lett.* **B356**, 329 (1995).
- [10] K. Binder, *Z. Phys. B* **43**, 119 (1981).
- [11] E.Luijten and H.W.J. Blöte, *Phys. Rev. Lett.* **76**, 1557 (1996); *ibid.* **76**, 3662 (1996); H.W.J. Blöte and E.Luijten, *Europhys.Lett.* **38**, 565 (1997); E.Luijten, *Europhys.Lett.* **37**, 489 (1997).
- [12] K.K.Mon, *Europhys.Lett.* **34**, 399 (1996); *ibid.* **37**, 493 (1997).
- [13] G.Parisi and J.J.Ruiz-Lorenzo, *Phys. Rev. B* **54**, R3698 (1996); **55**, 6082 (1997).
- [14] H.G.Ballesteros, L.A.Fernandez, V.Martin-Mayor and A. Munoz-Sudupe, *Phys. Lett. B* **441**, 330 (1998).
- [15] M.Hasenbusch, *J.Phys.A* **32**, 4851 (1999).
- [16] X.S.Chen and V.Dohm, *Int.J.Mod.Phys.* **C9**, 1073 (1998).
- [17] U. Wolff, *Phys. Rev. Lett.* **62**, 361 (1989).
- [18] A. M. Ferrenberg and R. H. Swendsen, *Phys. Rev. Lett.* **61**, 2635 (1988).
- [19] R.Guida and J.Zinn-Justin, *J.Phys.A* **31**, 8103 (1998).
- [20] E.Luijten, K.Binder, and H.W.J. Blöte, *Eur. Phys. J.* **B9**, 289 (1999).
- [21] H.Kawamura, *J.Phys.Condens.Matter* **10**, 4707 (1998).
- [22] E.Brezin,D.R.Nelson, and A.Thiaville, *Phys.Rev.* **B31**,7124 (1985).
- [23] X.Hu, S.Miyashita, and M.Tachiki, *Phys.Rev.Lett.* **79**,3498 (1997).
- [24] M. Itakura, *Phys. Rev. B* **60**, 6558 (1999).

FIGURES

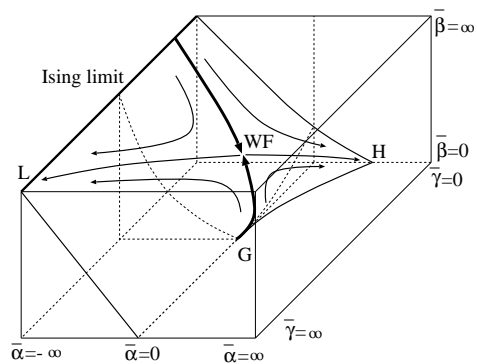


FIG. 1. Renormalization flow of regularized parameter in $D = 3$.

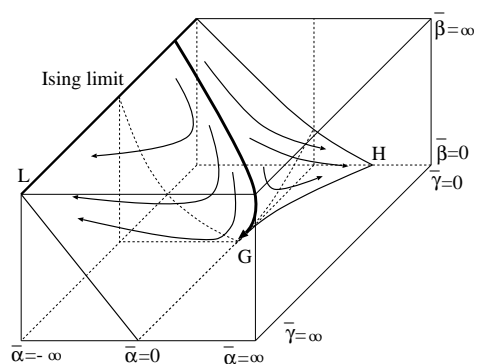


FIG. 2. Renormalization flow of regularized parameter in $D = 4$.

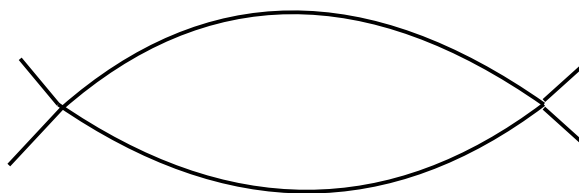


FIG. 3. Divergent subdiagram in $D = 4$.

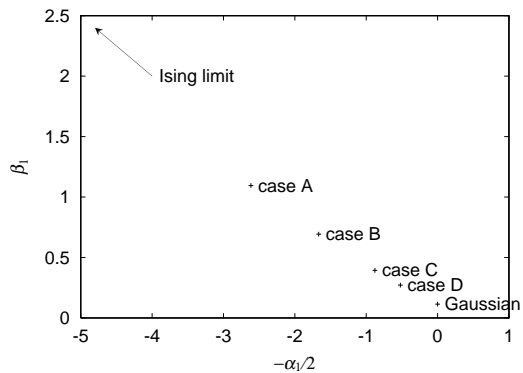


FIG. 4. Parameters at which simulations were performed.

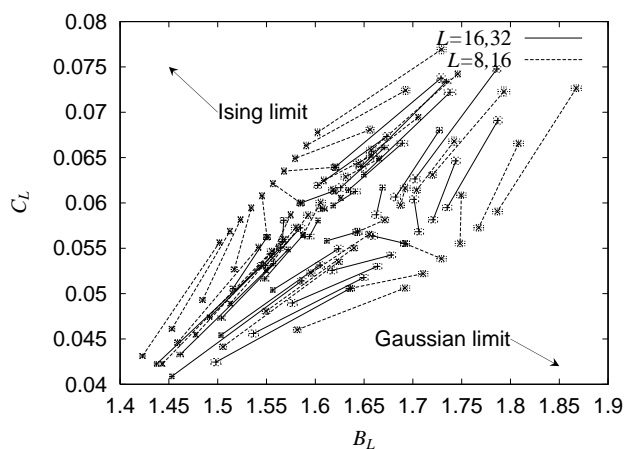


FIG. 5. RG flow near the Wilson-Fisher fixed point in $D = 3$. All lines are drawn from (B_L, C_L) to (B_{2L}, C_{2L}) .

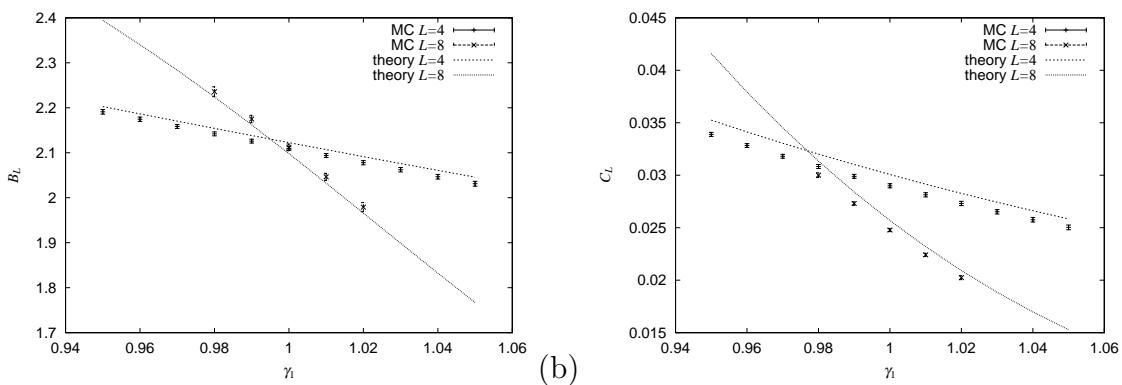


FIG. 6. Plot of (a) B_L and (b) C_L against γ_1 for the Case B in $D = 4$. “MC” denotes Monte Carlo result and “theory” denotes finite-size perturbation result.

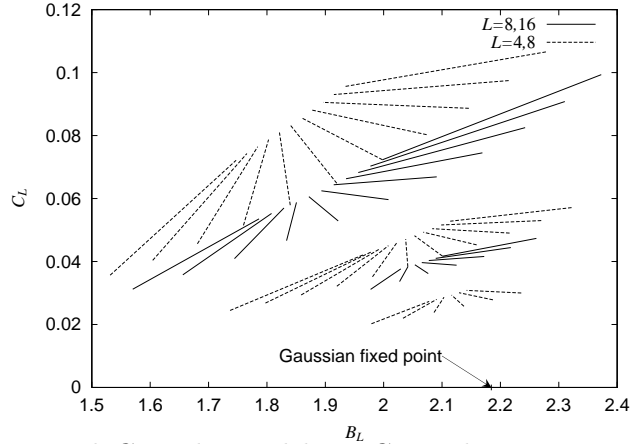


FIG. 7. RG flow of B_L and C_L , obtained by MC simulation in $D = 4$. All lines are drawn from (B_L, C_L) to (B_{2L}, C_{2L}) . Dashed and solid lines correspond to $L = 4$ and $L = 8$, respectively.